

# Segmenting Blood Vessels in Retinal Images using a Entropic Thresholding Scheme

Fabiola M. Villalobos-Castaldi, Edgardo M. Felipe-Riverón  
and Cecilia Albortante-Morato

Center for Computing Research, National Polytechnic Institute,  
Av. Juan de Dios Batiz and Miguel Othon de Mendizabal, Mexico, D.F.,  
P. O. 07738. México. Phone: 5729 6000/56515.  
fvillalobosb07@sagitario.cic.ipn.mx, edgardo@cic.ipn.mx, amoratob07@sagitario.cic.ipn.mx

**Abstract.** In this paper it is presented a fast and automatic method to segment and extract blood vessels from retinal images. The proposed method is based on the second local entropy and in the grey level co-occurrence matrix (GLCM). It is very helpful for the computation of a threshold the information that the GLCM has about the contours and the spatial distribution of the grey levels. Therefore, the algorithm is designed to have flexibility in the definition of the blood vessel contours, since it is able to fit the contours. Using the information of the GLCM a statistic feature is calculated which acts as a threshold value. The average time required for the propose method is 6 seconds. To asses the ability and speed of the proposed method, the experimental results are compared with the state-of-the-art results obtained by another methods.

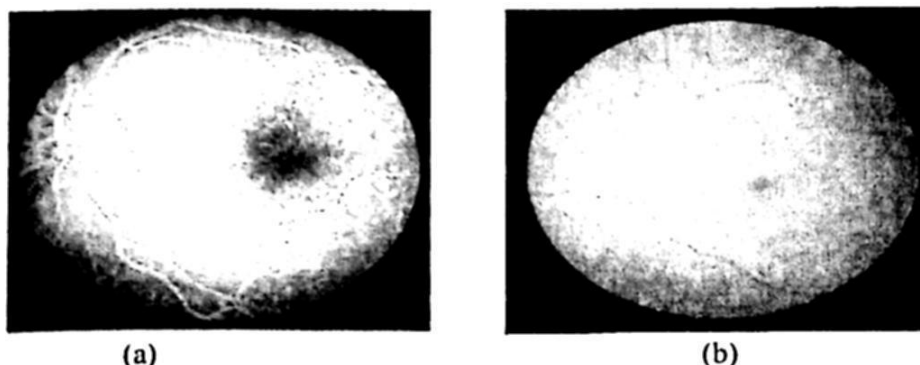
## 1 Introduction

The retina is the only place in humans where blood vessels can be directly visualized in a non-invasively in vivo way. Ophthalmic photography is a highly specialized form of medical imaging dedicated to the study and treatment of disorders of the eye. There are two common procedures to perform such photography: (a) angiography (Figure 1.a)) and (b) fundus photography (Figure 1.b)). Angiography is the imaging of vessels, and the resulting pictures are angiograms. Angiography of the retina of the eye requires the injection of a small amount of dye into a vein in the patient's arm. The dye travels through the blood stream and is photographed using special cameras and colored light in the meantime it travels through the vessels of retina. Fluorescein Angiography and Indocyanine Green (ICG) are the two main types of such procedure. Figure 1a.shows examples of ophthalmic photography.

Alternatively, when performing for ophthalmic fundus photography for diagnostic purposes, the pupil is dilated with eye drops and a special camera called a *fundus camera* is used to focus on the fundus. The resulting images are detailed and revealing, showing the optic nerve through which visual 'signals' are transmitted to the brain and the retinal vessels which supply nutrition and oxygen to the tissue.

Figure 1.1b shows an example of a digital fundus photograph, where the contrast between the blood vessels and retinal background is not as good as it is in fluorescein

angiogram. Fundus photographs are usually taken using a green filter ('red-free') to acquire images of retinal blood vessels, since green light is absorbed by blood and appear in the fundus photograph darker than the background and the retinal nerve fiber layer.



**Fig.1.** Examples of ophthalmic photography (a) Fluorescein angiogram (b) Digital fundus photograph.

Fluorescein angiography permits to detect and quantify changes in the blood vessels geometry more accurately than in fundus photography due to the high contrast between the blood vessel and the background retinal layer; it is bloody and sometimes unsuitable for certain people because of allergic reactions; thus fundus photography is more widely used in clinics. Despite the high resolution of photographs in fundus photography, the contrast between the blood vessels and retinal background tends to be poorer than that in angiograms.

Retinal or fundus images provide information about the blood supply system to the retina. Ocular fundus image assessment has been widely used by the medical community for diagnosing vascular and non vascular pathologies. Inspection of the retinal vasculature may reveal hypertension, diabetes, arteriosclerosis, cardiovascular disease and stroke [13]. For example, central retinal artery occlusion usually causes generalized constriction of retinal arteries. While central retinal vein occlusion typically produces dilated tortuous veins, arteriosclerosis can cause arteries to acquire a copper or silver color. Hypertension may result also in focal constriction of retinal arteries, and diabetes can generate new blood vessels (neovascularization). Among the features in ocular fundus image, the structure of retinal blood vessels plays an important role in revealing the state of retinal diseases. In addition, blood vessels can also serve as landmarks for image-guided laser treatment of choroidal neovascularization.

### 1.1 Fundus Image Analysis

Although the underlying mechanisms for some eye diseases are not fully understood, its progress can be prevented by early diagnosis and treatment. A number of steps is necessary to carry out such analysis. In general, it is necessary first to segment the blood vessels from the fundus image. Accurate blood vessel segmentation is fundamental in the analysis of fundus images since further analysis usually depends on the

accuracy of this segmentation. It allows a quantitative measurement of the geometrical changes of arteries, tortuosity or lengths, and provides the localization of landmark points such as bifurcations needed for image registration [8]. It is therefore desirable to provide ways of automating the process of the analysis of fundus images, using computerized image analysis, so as to provide at least preliminary screening information and also as an aid to diagnosis to assist the clinician in the analysis of difficult cases. Visually, vessels in the fundus image appear as dark lines on a relatively uniform bright background. Various methods are known for segmenting the fundus image. The aim of vasculature segmentation is to take a fundus image as input and create a new binary image of the complete vasculature as output. This output image contains the mask of the vascular structure. Only when the vascular mask has been created and the vessels have been detected, the analysis process can be done. Therefore, accurate vasculature segmentation is fundamentally important in the analysis of fundus images, as further analysis usually depends on the accuracy of this segmentation.

Segmentation methods vary depending on the imaging modality, application domain, method being automatic or semi-automatic, and other specific factors. While some methods employ purely intensity-based pattern recognition techniques such as thresholding followed by connected component analysis, other methods apply explicit vessel models to extract the vessel contours. Depending on the image quality and general image artifacts such as noise, segmentation methods may require image pre-processing before applying the segmentation algorithm. Other methods apply post-processing to overcome the problems of so called over-segmentation.

## **1.2 Characteristics of the Vasculature**

The vasculature has a number of characteristics that the image processor can exploit in developing a segmentation technique [6], [14], [3].

- ❖ The vessel cross-sectional gray level profile approximates a Gaussian shape.
- ❖ The vasculatures is piecewise linear, it can be represented by many connected line segments.
- ❖ The direction and gray level of a vessel do not change abruptly, they are continuous.
- ❖ The vasculature is tree-like; all vessels are connected to all other vessels and they all originate within a single area, the optic disc.
- ❖ Arterial vessels and venous vessels do not cross themselves independently.
- ❖ Every vessel crosses are between the arterial and venous branches.

Some factors that hinder vascular segmentation are:

- ❖ Vessels are obviously not all the same size, shape or color.
- ❖ The contrast can sometimes be low; the vessel color can be close to that of the background.
- ❖ Some background features have similar attributes as vessels.
- ❖ Vessels crossings and bifurcations can confuse some techniques.
- ❖ The optic disk can be wrongly segmented as a vessel.

### 1.3 Vasculature Segmentation Methods

Advances in vascular imaging technology have provided radiologist non-invasive imaging modalities that can give accurate vascular information, which helps the physician to define the character and extent of a vascular disease, aiding diagnosis and prognosis (Kirbas C., 2004). As stated previously, accurate vascular extraction is the primary task in automated ophthalmic image analysis. The existing vessel extraction techniques and algorithms can be classified into five main categories as follows:

1. Pattern recognition techniques,
2. Tracking-based approaches,
3. Artificial intelligence-based approaches,
4. Model-based approaches and,
5. Others

## 2 The Proposed Method

The proposed method in this paper uses one of the basic approaches to edge detection: the enhancement/thresholding method to achieve a fast algorithm for automated detection of blood vessels in retinal images.

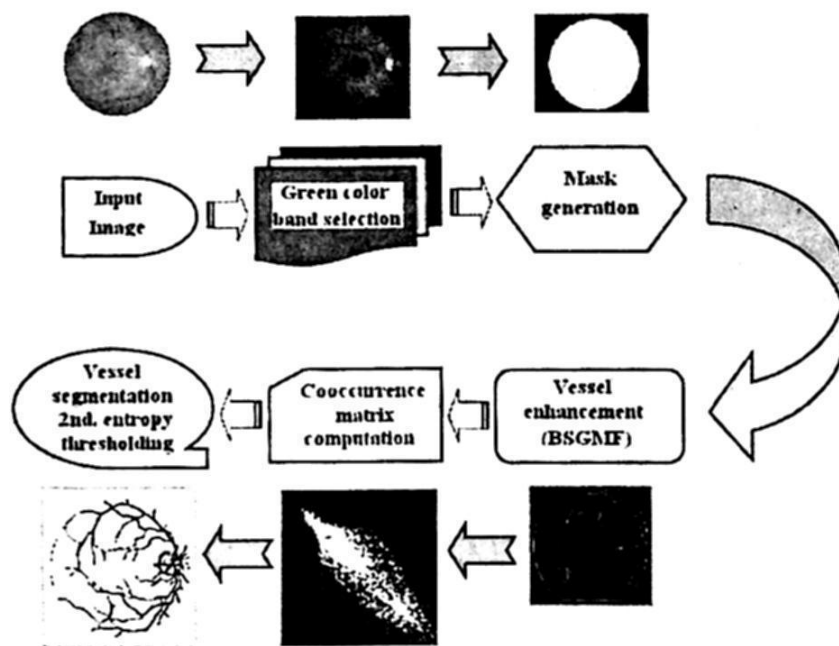


Fig. 2. Block diagram of the proposed method.

As depicted in Figure 2, our method follows four main steps: 1) automatic mask generation to avoid processing of the black border and corners present in images; 2) application of a matched filter to enhance the vessels edges; 3) computation of the co-occurrence matrix; and 4) automatic vessel network segmentation using the second order entropy.

## 2.1 Mask Generation

Mask generation aims at labeling pixels belonging to the fundus Region of Interest (ROI) in the entire image. Pixels outside that ROI are those belonging to the dark surrounding region in the image. Those pixels are not strictly dark (zero intensity value) and the need to discard them for subsequent processing stages are necessary. The mask generation uses a thresholding with a free parameter empirically chosen such that pixels with intensity value above that threshold are considered to belong to the ROI. The threshold is applied in the green color band of the image (Figure 3).

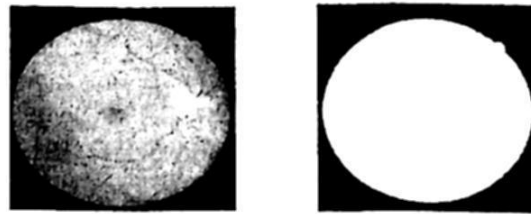


Fig. 3. Example of mask generation

The algorithm is robust enough to allow automatic mask generation in images of low visual quality, which is the principal issue in this step. All images of our dataset were correctly masked with this process.

## 2.2 Enhancement of Blood Vessels by Belt-Shape Gaussian Matched Filters

It can be noted that the retina vessels can be represented by piecewise linear segments with Gaussian-shaped cross sections. A matched filter is constructed for the detection of the vessel edge segments searching in all possible directions. Gray-level values of a blood vessel cross section can be approximated by a Gaussian curve (Eq. 1):

$$f(x, y) = A \left[ 1 \pm K \exp\left(-\frac{d^2}{2\sigma^2}\right) \right] \quad (1)$$

Where  $d$  is the perpendicular distance between the pixel at  $(x, y)$  and the centerline of the blood vessel,  $\sigma$  defines the spread of the intensity profile,  $A$  is the gray-level intensity of the local background, and  $K$  is a constant used to account for the reflectance of the blood vessel relative to its neighborhood.

Based on Eq. (1), Chaudhuri [2] derived a 2-D Gaussian  $\theta$  angle matched filter kernel given by (Eq. 2):

$$K_{\theta}(x, y) = \pm \exp\left(-\frac{u^2}{2\sigma^2}\right) \quad (2)$$

Where  $(u, v)^T$  is a new coordinate of  $(x, y)^T$  after that  $(x, y)^T$  is rotated by a  $\theta$  angle. In other words, if we let  $R(\theta)$  be the rotation matrix specified by  $\theta$ , then:

$$R(\theta) = \begin{bmatrix} \cos \theta & -\sin \theta \\ \sin \theta & \cos \theta \end{bmatrix} \tag{3}$$

And  $(u, v)^T = (x, y)^T R(\theta)$ . Chaudhuri et al., 1989, used Eq. (2) to design 12 2-D Gaussian  $\theta$  angle-matched filter kernels  $\{K_\theta(x, y)\}_{i=0}^{11}$  to cover 12 orientations of a blood vessel in angles  $\theta_0 = 0^\circ, \theta_1 = 15^\circ, \dots, \theta_{11} = 165^\circ$ , where the difference between two consecutive angles is 15 deg., i.e.,  $\theta_{i+1} - \theta_i = 15^\circ$ .

One drawback of the approach of Chaudhuri et al., 1989, is the high computational complexity. It requires separate implementations of 12 kernels  $\{K_\theta(x, y)\}_{i=0}^{11}$ . To mitigate these problems, a bell-shaped Gaussian matched filter (BSGMF) was developed to cover all 12 orientations where designed kernel was given by [9] (Eq. 4).

$$K(x, y) = \pm \exp\left(-\frac{x^2 + y^2}{2\sigma^2}\right) \tag{4}$$

With the tail truncated at  $x^2 + y^2 = 3\sigma^2$ . Equation (4) is not a low-pass filter, but rather a bell-shaped Gaussian filter. As noted in [2], it was an effective filter to detect bell-shaped objects. Since the new kernel has a Gaussian shape along every direction that makes it look like a bell, it is named the BSGMF.

### 2.3 Computation of the Co-occurrence Matrix

Given a digital image of size  $M \times N$  with  $L$  gray levels denoted by  $G = \{0, 1, \dots, L-1\}$ , let  $f(x, y)$  be the gray level of the pixel at the spatial location  $(x, y)$ . Then the image can be represented by a matrix  $F = [f(x, y)]_{M \times N}$ . A co-occurrence matrix of an image is an  $L \times L$  square matrix, denoted by  $W = [t_{ij}]_{L \times L}$ , where  $t_{ij}$  is the number of transitions from gray level value  $i$  to gray level value  $j$  defined as follows [9], [10]:

$$t_{ij} = \sum_{m=1}^M \sum_{n=1}^N \delta_{mn} \tag{5}$$

With

$$\delta_{mn} = 1$$

If

$$\begin{cases} f(m, n) = i, \text{ and } f(m, n+1) = j \\ \text{and / or} \\ f(m, n) = i, \text{ and } f(m+1, n) = j \end{cases} \tag{6}$$

= 0 Otherwise

Each entry in the matrix  $t_{ij}$  (Eq. 5) gives the number of times the pixel gray level  $j$  follows the gray level  $i$  in some pattern. Depending upon different patterns, then

different definitions of co-occurrence matrix are possible. It has been reported in [4] and [10] that consideration of both horizontal and vertical transitions allows all the edges to participate in the threshold selection. Note that the co-occurrence matrix just defined in (6) considers only the pixel transition to the right as well as to below since it has been found that including the pixels on the left and above the transition does not provide significant information and improvement.

Normalizing the total number of transitions in the co-occurrence matrix, a desired transition probability from gray level  $i$  to  $j$  is obtained by

$$P_{ij} = \frac{t_{ij}}{\sum_{k=0}^{L-1} \sum_{l=0}^{L-1} t_{kl}} \quad (7)$$

If  $t$ ,  $0 \leq t \leq L-1$ , is a threshold, then " $t$ " partitions the co-occurrence matrix into four quadrants, namely, A, B, C and D as seen in Figure 4.

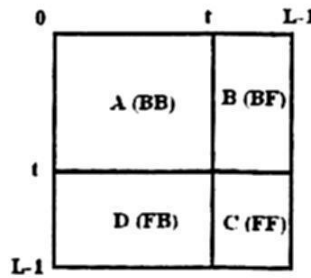


Fig. 4. Quadrants of the co-occurrence matrix.

These four quadrants can be further grouped into two classes. If we assume that pixels with gray levels above the threshold are assigned to the foreground (vessel), and those with gray levels equal to or below the threshold are assigned to the background, quadrants A and C correspond to local transitions within background (B), denoted by BB and foreground (F), denoted by FF, respectively, as shown in Figure 4.

Similarly, quadrants B and D represent transitions across boundaries between background and foreground, thus, they can be denoted by BF and FB, respectively. Thus, if we let  $G_0 = \{0, \dots, t\}$  and  $G_1 = \{t+1, \dots, L-1\}$ , the four quadrants A(BB), B(BF), D(FB), and C(FF) are determined by the gray-level ranges  $G_0 \times G_0$ ,  $G_0 \times G_1$ ,  $G_1 \times G_0$ ,  $G_1 \times G_1$ , respectively. Then the probabilities associated with each quadrant can be obtained by:

$$P'_A = \sum_{i=0}^t \sum_{j=0}^t P_{ij} \quad P'_B = \sum_{i=0}^t \sum_{j=t+1}^{L-1} P_{ij} \quad (8)$$

Normalizing the probabilities within each individual quadrant, such that the sum of the probabilities of each quadrant equals one, we get the cell probabilities for different quadrants. In the case of the first quadrant (Eq. 9 and Eq.10):

$$P_{ij}^A = \frac{P_{ij}}{P_A} = \frac{t_{ij}}{\sum_{i=0}^t \sum_{j=0}^t t_{ij}} \quad (9)$$

$$= \frac{t_{ij}}{\sum_{i=0}^t \sum_{j=0}^t t_{ij}} \quad (10)$$

For  $0 \leq i \leq t, 0 \leq j \leq t$

Similarly,

$$P_{ij}^B = \frac{P_{ij}}{P_B} = \frac{t_{ij}}{\sum_{i=0}^t \sum_{j=t+1}^{L-1} t_{ij}} \quad (11)$$

$0 \leq i \leq t, t+1 \leq j \leq L-1$

And

$$P_{ij}^C = \frac{P_{ij}}{P_C} = \frac{t_{ij}}{\sum_{i=t+1}^{L-1} \sum_{j=t+1}^{L-1} t_{ij}} \quad (12)$$

$t+1 \leq i \leq L-1, t+1 \leq j \leq L-1$

$$P_{ij}^D = \frac{P_{ij}}{P_D} = \frac{t_{ij}}{\sum_{i=t+1}^{L-1} \sum_{j=0}^t t_{ij}} \quad (13)$$

$t+1 \leq i \leq L-1, 0 \leq j \leq t$

## 2.4 Segmentation

Segmentation is the technique and procedure used to divide an image into non-overlapping different regions according to their particular characteristics. The pixel values in the same segmented region have similar attributes, but the pixel values between different regions have dissimilar attributes. Thresholding is a method commonly used in segmentation and is the foundation of other segmentation methods [10]. In recent years, in order to reduce the information loss during the segmentation



process, an information theory method has been introduced into experimental segmentation.

For example, based on 1D entropy method, an image can be divided into two parts according to the threshold value obtained from the 1D entropy. Once the entropy of each one of the two parts is equal or approximately equal, the value of 1D entropy will reach the maximum and the automatic segmentation will be realized. Compared to 1D entropy, 2D entropy can reflect not only the information of pixel gray value, but also the statistical rule of two pair of pixels between fixed-position in the image. Thus, the 2D entropy has been widely utilized. The first step of 2D segmentation is to build the 2D histogram, which can be commonly established by using the gray-level gradient co-occurrence matrix.

#### 2.4.1 1D Entropy

Let  $X$  be a discrete random variable and its probability distribution  $p_i = \{X = x_i\}$ ,  $i = 1, 2, \dots, n$ , then the 1D entropy can be defined as follows (Eq. 14):

$$H(X) = -\sum_{i=1}^n p_i \log p_i \quad (14)$$

Where  $\{x_1, x_2, \dots, x_n\}$  is a sample of random variable  $X$ , and the base of logarithm could be 2, 3 or 10.

#### 2.4.2 2D Entropy

Now, the second order local entropy of the background can be defined as:

$$H_A^{(2)}(t) = -\frac{1}{2} \sum_{i=0}^t \sum_{j=0}^t P_{ij}^A \log_2 P_{ij}^A \quad (15)$$

Similarly the second order entropy of the object can be written as:

$$H_C^{(2)}(t) = -\frac{1}{2} \sum_{i=t+1}^{L-1} \sum_{j=t+1}^{L-1} P_{ij}^C \log_2 P_{ij}^C \quad (16)$$

Hence the total second order local entropy of the object and the background can be written as:

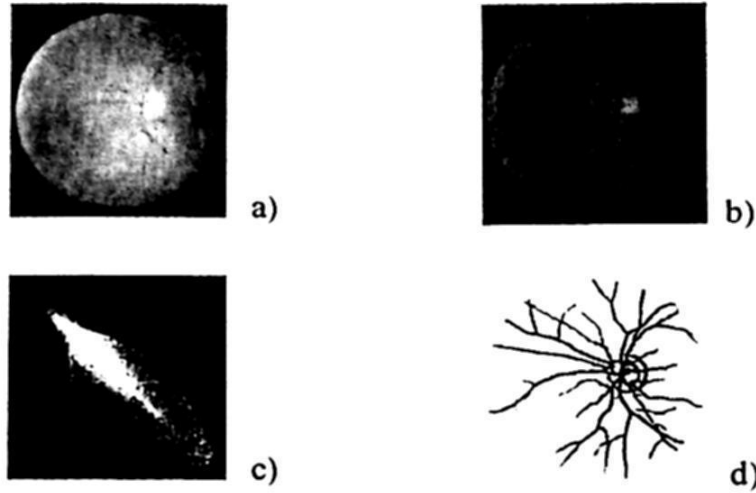
$$H_T^{(2)}(t) = H_A^{(2)}(t) + H_C^{(2)}(t) \quad (17)$$

The gray level corresponding to the maximum of  $H_T^{(2)}(t)$  gives the threshold for object-background segmentation.

$$t = \text{Arg} \left\{ \max_{0 \leq t \leq L-1} H_T^{(2)}(t) \right\} \quad (18)$$

### 3 Experimental Results

In this paper we used the images included in the well-known DRIVE database to assess the performance of the proposed method [11].



**Fig. 5.** Steps of the segmentation process for a typical image. a) Original image. b) Green color band used for the enhancement process. c) Co-occurrence matrix obtained and the corresponding threshold (Red cross). d) Segmented vessel and the elapsed time to get it.

The DRIVE database contains 40 color images, which were captured in digital form from a Canon CR5 non-mydratic 3CCD camera at 45° field of view (FOV). The images are of size 565 × 584 pixels, 8 bit per color channel. The images have been divided into 2 sets. A training set and a test set. Each one contains 20 color retina images. Each set also contains the corresponding segmented images, which were graded by two experts (called first observer and second observer). Images in the training set were graded only once, and were named from 21\_manuall to 40\_manuall. The images in the test set were graded by the two specialists, and the segmented images were named as 1\_manuall to 20\_manuall, and 1\_manual2 to 20\_manual2. The total amount of segmented images in the database is 60, 20 in the training set and 40 in the test set.

#### 3.1 Execution Time

Finally, we focus the analyses on the time that the proposed algorithm takes out to accomplish the whole process for blood vessel segmentation. On a Pentium 4, CPU 1.73GHz, with a MATLAB 7.4.0 (R2007a) implementation, it takes as average 6 seconds to obtain the image with the segmented vessels. Table 1 shows the elapsed time comparison amongst our method with some state-of-the-art results obtained from [2], [12], [1] and [5]. The execution time required for each step is illustrated in Table 1.

**Table 1.** Comparison of the execution times.

<b>Method</b>	<b>Execution Time</b>
Manual	2 hr
Yiming Wang [12]	7.0 min
Soares JVB [5]	3.0 min
T. Chanwimaluang [1 ]	2.5 min
S. Chaudhuri [2 ]	1.0 min
<b>Villalobos and Felipe</b>	<b>6.2 s</b>

**Table 2.** Execution time of each step.

<i>No. of the step</i>	<i>Step</i>	<i>Execution time (seconds)</i>
1	Green color band separation	0.1453
2	Enhancement	5.5400
3	Mask generation	0.2000
4	Vessel segmentation	0.3200
	<b>Total</b>	<b>6.2053</b>

As it can be seen, the most time-consuming process is the enhancement step where the BSGMF is applied, and the segmentation step based on the second local entropy thresholding. Figure 6 illustrates the results of some of the segmented vessel images and the elapsed time required to get each of them.

#### 4 Conclusions

In this paper we presented a pixel processing approach for the fast automatic detection and extraction of retinal vessels from retinal fundus images using a thresholding method based on the second local entropy and in the gray level co-occurrence matrix (GLCM). Using one of the approaches of the edge detection, the enhancement/thresholding, the proposed method reduced the time required for extracting and segmenting the retinal vessel of fundus images without reducing the accuracy. In most of the methods, the time is not a normal relevant aspect to evaluate, in spite its importance when we deal with a huge image data base. That is why we focus also in this aspect. The average time required to segment the complete vessels is 6 seconds. Based on these results we consider that our method offers a good alternative for those applications where the time of analysis plays an important role.

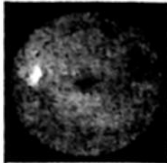

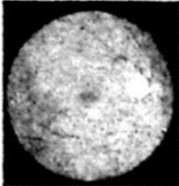

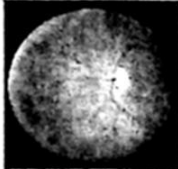

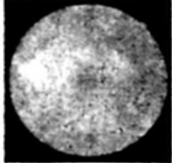

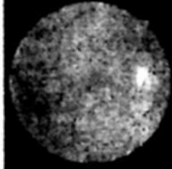

Original image	Segmented vessel	Elapsed time (seconds)
		6.73
		6.004
		6.051
		6.41
		6.343

Fig. 6. Original image, the segmented vessel image and the elapsed time for some images.

**Acknowledgements.** The authors of this paper wish to thank the Computing Research Center (CIC), Mexico; Postgraduate and Research Secretary (SIP), Mexico, under research grant 20082213, and National Polytechnic Institute (IPN), Mexico, for their support.

## References

1. Chanwimaluang T. and Fan G., (2003), An efficient blood vessel detection algorithm for retinal images using local entropy thresholding. In: *Proc. of the IEEE Intl. Symp. on Circuits and Systems*.
2. Chaudhuri S., Chatterjee S., Katz N., Nelson N., and Goldbaum M., (1989), Detection of Blood Vessels in Retinal Images Using Two-Dimensional Matched Filters, *IEEE Transactions on Medical Imaging*, 8(3):263–269.
3. Matsopoulos G. K., Mouravliansky N.A., Delibasis K.K. and Nikita K.S., (1999), Automatic retinal image registration Scheme using global optimization techniques, *IEEE Trans. Information technology in biomedicine*, vol. 3.

4. Pal N.R., Pal S.K., (1989), Entropic thresholding, *Signal Process* 16, 97-10.
5. Soares JVB, Leandro JJG, Cesar RM, Jelinek HF, and Cree MJ., (2006), Retinal vessel segmentation using the 2-D Gabor wavelet and supervised classification, *IEEE Transactions on Medical Imaging*, 25:1214-1222.
6. Zana F. and Klein J. C., (1997), Robust Segmentation of Vessels from Retinal Angiography. In *International Conference on Digital Signal Processing*, pages 1087-1091, Santorini, Greece.
7. Kirbas C. and Quek (2004), A review of vessel extraction techniques and algorithms, *ACM Comput. Surv.*, 36(2):81-121.
8. Badrinath Roysam, Kenneth H. Fritzsche, Charles V. Stewart, (2002), Doctoral Dissertation, *Computer Vision Algorithms for Retinal Vessel Width Change Detection and Quantification*, Department of Electrical, Computer, and Systems Engineering Rensselaer Polytechnic Institute.
9. Ching-Wen Yang, Dye-Jyun Ma, Shuenn-Ching Chao, Chuin-Mu Wang, Chia-Hsin Wen, Chien-Shun Lo, Pau-Choo Chung, Chein-I Chang, (2000), Computer-aided diagnostic detection system of venous beading in retinal images, *Society of Photo-Optical Instrumentation Engineers*. 39(5) 1293-1303.
10. Zhang Y F, and Zhang Y, (2006), Another Method of Building 2D Entropy to Realize Automatic Segmentation, *International Symposium on Instrumentation Science and Technology; Journal of Physics: Conference Series* 48, 303-307.
11. Wang L. and Bhalerao A., (2003), Model Based Segmentation for Retinal Fundus Images. In *Proc. of Scandinavian Conference on Image Analysis (SCIA)*.
12. Niemeijer M., Staal M., J. van Ginneken J., van, Loog M B. B. and. Abraamoff M. D., (2004), Comparative study of retinal vessel segmentation methods on a new publicly available database, *Sciences Institute* at <http://www.isi.uu.nl/Research/Databases>.